Full Papers
doi.org/10.1002/ejoc.202001475

Chemistry Europe
European Chemical Societies Publishing

Tris(5-aryl-1,3,4-oxadiazolyl)benzotrithiophenes – Discotic Liquid Crystals with Enormous Mesophase Ranges

Natalie Tober,[a] Johannes Winter,[a] Matthias Jochem,[a] Matthias Lehmann,*[b] and Heiner Detert*[a]

Dedicated to the memory of Prof. Dr. Klaus Banert (1955–2020).

C_3-symmetrical, alkoxyphenyl substituted 2,5,8-(tris-1,3,4-oxadiazol-2-yl)benzo [1,2-b; 3,4-b′; 5,6-b″]trithiophenes (OXD-BTT) are synthesized via threefold Huisgen-reaction. A broad variation of alkoxy substitution pattern and chain lengths is reported. The thermal behavior was investigated via differential scanning calorimetry (DSC), polarized optical microscopy (POM) and thermogravimetry (TGA). Optical properties were studied via UV-Vis and fluorescence spectroscopy. Structural information of the LC phases was gained from X-ray diffraction on oriented fibers. OXD-BTT provide enormous phase widths ($\Delta T \geq 289$ K) with clearing points close to thermal decomposition. Most of the derivatives exhibit two different mesophases, the lower phase with a rectangular 3D-structure and a hexagonal 2D-lattice at higher temperature. The variation of the chain length allows a tuning of melting and clearing points. OXD-BTT emit blue light with fluorescence quantum yields up to 30% in good solvents. The emission is very sensitive to aggregation, thus, in poor solvents the emission intensity decreases, and red shift of maxima occurs.

Introduction

Thiophene is a building block of utmost importance for the synthesis of organic electronic materials.[1] A large variety of oligo- and polythiophenes have been prepared and successfully applied as active material in electronic devices, e.g. OLEDs, OFETs, OVPs and sensors.[1a,2] Polythiophenes have good charge carrier mobilities.[1a–e,3] PEDOT, especially in combination with polystyrene sulfonic acid, is produced in large quantities and is used for a broad scope of applications, in capacitors, as transparent electrodes, or as electrochromic material.[4] One challenge in plastic electronics is the alignment of the polymers within the conductive layer. Jiang et al.[1a,f] presented a brilliant approach, the targeted electrochemical polymerization on the electrode, constraining the π-systems to be optimally aligned.

Another strategy for orientation and targeted alignment of electronic materials is based on the self-assembly of large aromatic molecules to form conductive columns.[5] Discotic liquid crystals (DLCs) are the prime material for this purpose, they also offer self-healing properties. Triphenylenes are probably the best investigated class of DLCs,[6] but related discs[2e,l,7] and even star-shaped π-systems[8] are emerging electronic materials. The cyclic trimer of thiophene, benzotrithiophene (BTT), a C_3-symmetrical disc, has good stacking properties but poor to moderate solubility. In single crystals of BTT derivatives, charge carrier mobilities up to $\mu = 0.14\ cm^2 V^{-1} s^{-1}$ can be generated due to the ideal π-π stacking;[1b,3a] linking alkyl chains to the periphery greatly enhances the solubility. Until now, only the groups of Eichhorn, Perepichka, and Grozema have investigated the modification of the periphery of BTT-derivatives for forming liquid crystals.[3a,5a,b] They investigated a triamide with impressive width of the mesophase of up to $\Delta T = 289$ K, a high thermal stability, and electronic properties such as charge carrier mobilities of $\mu = 0.002\ cm^2 V^{-1} s^{-1}$ and a HOMO-LUMO gap of $\Delta H = 3.45$ eV. The characteristics make liquid crystals with a BTT core a fascinating field of research. The reported OXD-BTTs consist of a thiophene core, which is attached to three oxadiazole units. Oxadiazoles are typical units in electron deficient π-conjugated materials.[9] As the 2,5-diaryl-substituted 1,3,4-oxadiazole has an opening angle of 134°, the geometry of π-systems comprising this unit is significantly bent, donor-acceptor interactions with neighboring electron-rich arenes planarize the molecules.[10] While the 134° opening angle of 1,3,4-oxadiazoles hampers their use as building blocks of calamitic LCs, they are currently used to build banana-shaped and hockey-stick liquid crystals[11] and also successfully in the formation of discotic mesogens.[12] The oxadiazoles can act as electron acceptors in electron-deficient materials for electronic devices. Furthermore, liquid crystalline oxadiazoles often show medium to high fluorescence quantum

[a] Dr. N. Tober, J. Winter, M. Jochem, Prof. Dr. H. Detert
Department of Chemistry
University of Mainz
Duesbergweg 10–14, 55128 Mainz, Germany
E-mail: detert@uni-mainz.de
Homepage: www.blogs.uni-mainz.de/fb09ak-detert/
[b] Prof. Dr. M. Lehmann
Institute of Organic Chemistry
University of Würzburg
Am Hubland, 97074 Würzburg, Germany
Homepage: www.chemie.uni-wuerzburg.de/oc/m-lehmann-group

Supporting information for this article is available on the WWW under https://doi.org/10.1002/ejoc.202001475

yields and are therefore also of interest for (non-linear) optical applications.[13] In continuation of a project on star-shaped materials,[9d,14] we report here luminescent discotic π-systems composed of a central BTT disc with alkoxyaryl-1,3,4-oxadiazole arms. All, except **8**, are discotic liquid crystals with broad mesophases. Optical properties such as solvatochromism in absorption and fluorescence, fluorescence quantum yields and aggregation-dependent emission are reported. A single crystal analysis of **8** gives proof of molecular structure and the thermotropic behavior has been investigated by polarization microscopy and differential scanning calorimentry. For selected representative examples the order in the liquid crystalline phase was additionally analyzed by X-ray diffraction on oriented fibers.

Results and Discussion

Synthesis

A retrosynthetic analysis of C_3-symmetrical tris(aryloxadiazolyl)-benzotrithiophenes OXD-BTT gives the construction of the oxadiazoles or connection of them to the BTT core as final and convergent step.

Among the different approaches to trisubstituted BTTs,[1f,15] Perepichkas high-yielding route (Scheme 1) leads straightforward to BTT-tricarboxylic acid,[1f,5b] an ideal reactant for the formation of oxadiazoles. Starting with 1,3,5-trichlorobenzene **1**, threefold Friedel-Crafts alkylation with chloroform under pressure[1f,16] yields 1,3,5-trichloro-2,4,6-tri (dichloromethyl)benzene **2** (Scheme 1). This is hydrolyzed in concentrated sulfuric acid in the presence of iron sulfate to form trialdehyde **3**. The subsequent nucleophilic substitution with ethyl mercaptoacetate, catalyzed by triethylamine, is followed by threefold Knoevenagel condensation to yield the tetracyclic triethyl benzo[1,2;3,4;5,6]tri(thiophene-2′-carboxylate) **4**. The BTT-ester can then be saponified to the desired carboxylic acid **5**.

The Huisgen reaction (Scheme 2) of carboxylic acid chlorides and 5-aryltetrazoles **7** is a mild and high-yielding method to construct extended π-systems with diaryl-1,3,4-oxadiazole units.[17] The convergent step of this route, had to be modified due to the insolubility of the acid chloride **6** even in aromatic solvents at elevated temperatures. Carboxylic acid **5** was suspended in thionyl chloride and stirred for 2d at 75 °C. Excess reagent was removed by distillation and **6** was suspended in abs. toluene at 80 °C. Addition of the respective tetrazole and collidine results in the formation of the tetrazolide followed by elimination of nitrogen and ring closure to 1,3,4-oxadiazoles. The thus formed alkoxy-substituted OXD-BTTs **8**–**17** were obtained in 24–80 % yield and nearly all are thermotropic liquid crystals (Table 1). Loss of material was mainly due to excessive chromatographic purification for removal of traces of by-products.

Alkoxyaryltetrazoles, the counterparts for the Huisgen reaction, are successfully prepared by two different synthetic strategies.[9d,14c,18] The 3,4-substituted derivatives were obtained by alkylation of 3,4-dihydroxybenzonitrile and subsequent 1,3-dipolar cycloaddition of azide to yield tetrazoles **7** (R^3=H, R^1=R^2=O-alkyl). The 3,4,5-substituted derivatives were synthesized via alkylation of gallic acid ester, saponification, chlorination and ammonolysis of the acid chlorides to amides followed by dehydration/azide addition with a reagent formed *in-situ* from silicon tetrachloride and sodium azide.[SI] Some of the so formed tetrazoles have recently been reported.[9d,14] Table 1 collects the BTT stars prepared by this procedure.

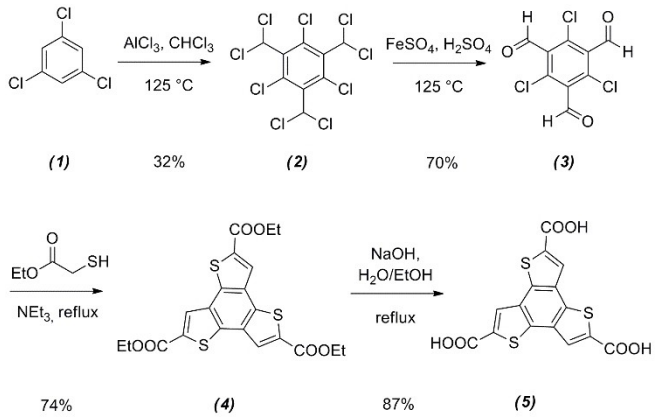

Scheme 1. Synthesis route of the BTT-core.

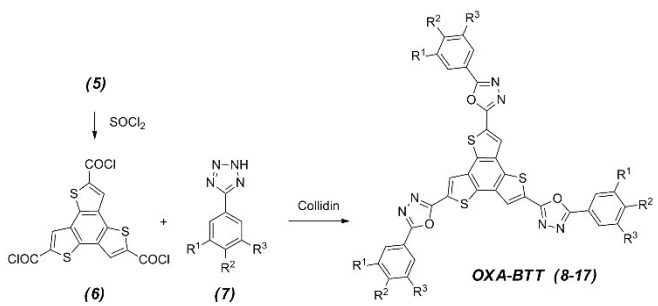

Scheme 2. Synthesis of OXD-BTT-compounds.

Table 1. Substitution pattern (Scheme 1), yields and liquid crystalline character of Tris-(alkoxyphenyl-1,3,4-oxadiazolyl)-BTTs.

Entry	R^1	R^2	R^3	Yield	LC
8	H	OC_3H_7	H	55 %	no
9	$OC_{10}H_{21}$	$OC_{10}H_{21}$	H	29 %	yes
10	$OC_{12}H_{25}$	$OC_{12}H_{25}$	H	70 %	yes
11	$OC_{14}H_{29}$	$OC_{14}H_{29}$	H	34 %	yes
12	OC_6H_{13}	OC_6H_{13}	OC_6H_{13}	80 %	yes
13	OC_8H_{17}	OC_8H_{17}	OC_8H_{17}	27 %	yes
14	$OC_{10}H_{21}$	$OC_{10}H_{21}$	$OC_{10}H_{21}$	24 %	yes
15	$OC_{12}H_{25}$	$OC_{12}H_{25}$	$OC_{12}H_{25}$	59 %	yes
16	$OC_{14}H_{29}$	$OC_{14}H_{29}$	$OC_{14}H_{29}$	40 %	yes
17	$OC_{16}H_{33}$	$OC_{16}H_{33}$	$OC_{16}H_{33}$	36 %	yes

Single Crystals

Single crystals (Figure 1) of **8** were obtained from a solution in *o*-dichlorobenzene at 179 °C. **8** crystallizes in a triclinic (P-1) lattice, the cell parameters are $a = 12.2$ Å, $b = 12.3$ Å, $c = 15.2$ Å, $\alpha = 81.1°$, $\beta = 75.0°$, $\gamma = 64.3°$ and the unit cell contains two molecules.[19]

Contrary to the aryloxadiazolyl arms, the central BTT unit shows disorder (balls in Figure 1A) of 18% regarding the orientation of the thiophene rings. The whole molecule is almost planar (Figure 1C), the additive torsion angles along the arms are less than 12°. In one of the three arms the propyl chain is coiled, and the methyl group points out of the molecular plane. The orientation of the one arm breaks the C_3-symmetry and the π-system adopts a "Y" shape. This deviation from higher symmetry appears frequently in three-armed stars and the disorder in thiophene orientation has been observed in annulated BTTs.[20]

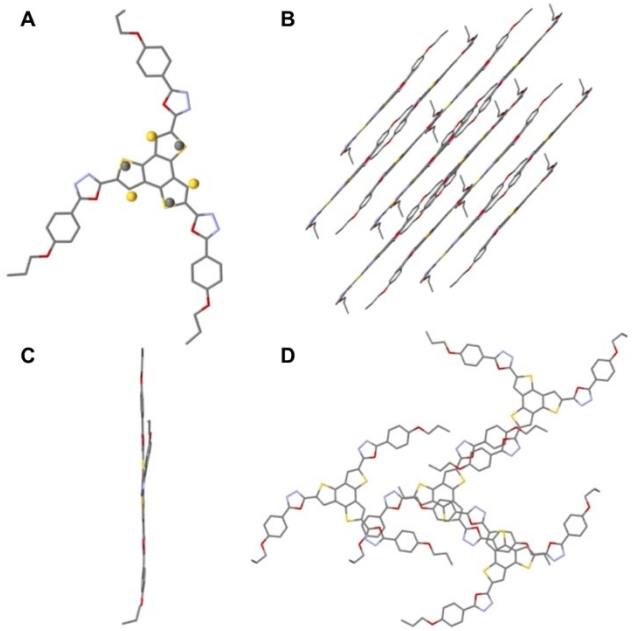

Figure 1. Single Crystal of OXD-BTT **8** (A) disorder in sulfur positions (balls); (B) layer structure; (C) planarity of OXD-BTT and (D) aromatic interactions.

The planar molecules are deposited in a layer structure (Figure 1B) with a spacing of 3.5 Å. Whereas several attractive π-π-interactions (Figure 1D) between thiophenes and oxadiazoles and between oxadiazoles and benzenes are observed, interactions between the individual BTT nuclei and significant sulfur-sulfur contacts are missing due to the high lateral shift of the nuclei to each other.

General mesomorpous behavior of 9–17

The BTT stars **9**–**17** have two different structured mesophases and clear between 240 °C and 328 °C (Table 2) with small enthalpy values, typical for LC materials. Most are thermally stable until clearing. TGA verifies thermal stability of **9**–**17** to 325 °C, only 2% weight loss was found up to 365 °C (TGA, SI). For example, the 3,4,5-tridecyl (short chain) derivative **14** has a clearing point at $T_c = 328$–336 °C (POM), a partial, concomitant decomposition of the sample was observed. The areas with decomposed substance are clearly visible under POM (*vide infra*, Figure 3C). For better illustration, the phase widths have been summarized in Figure 2.

The 3,4,5-derivatives **12**–**17** show a complex relationship of phase widths and chain length. They can essentially be classified into short chain (C6: **12**, C8: **13**, C10: **14**) and long chain (C12: **15**, C14: **16**, C16: **17**) compounds: with or without a typical melting point (DSC, Table 2). While **15**–**17** (with long chains) melt at about room temperature with high melting enthalpies $\Delta H > 25$ kJ mol^{-1}, **12**–**14** (with short chains) show no melting points, but rigidize in a highly ordered mesophase upon cooling. The high melting enthalpies are mainly caused by melting of the semi-crystalline alkyl chains. Thus **15**–**17** behave like classical, thermotropic liquid crystals. The 3,4-derivatives **9**–**11** do not show a melting signal in their DSC-thermograms, analogous to **12**–**14**. Crystallization for **9**–**14** was not observed by DSC, even after prolonged storage (9 months). Furthermore, all BTT stars show additional DSC transitions at medium temperatures with $\Delta H \leq 5$ kJ mol^{-1}(**9**–**11**: $T \approx 155$ °C, **12**–**14**: $T \approx 95$ °C, **15**–**17**: $T \approx 135$ °C; Table 2). The transitions of **9**–**14** can be regarded as a 3D organized mesophase, a soft crystalline phase or CONDIS crystal[21] or a rigidized highly ordered LC phase. The low transition enthalpies ($\Delta H \leq$

Table 2. Transition temperatures and enthalpies (values from 2nd heating scan).[a]

Entry	T [°C] Cr→M	ΔH [kJ mol^{-1}]	T [°C] M→M	ΔH [kJ mol^{-1}]	T [°C] M→I	ΔH [kJ mol^{-1}]
9			174	3.5	260	2.2
10			150	0.3	245	2.3
11			149	0.7	254[b]	3.5
12			95	3.3	325[b,c] dec.	
13			87	5.3	330[b,c,d] dec.	
14			99	0.8	328[d] dec.	
15	−2	26.9	130	10.7	289	14.3
16	20	57.3	147	5.7	273	10.7
17	49	154.3	156	3.6	240	8.8

[a] Cr: crystalline, M: mesomorphous, I: isotropic; [b] TGA **11**,**12**: decomposition starts at 325 °C, 2% weight loss at 365 °C; [c] no clearing point, dec.= decomposition, [d] POM observation.

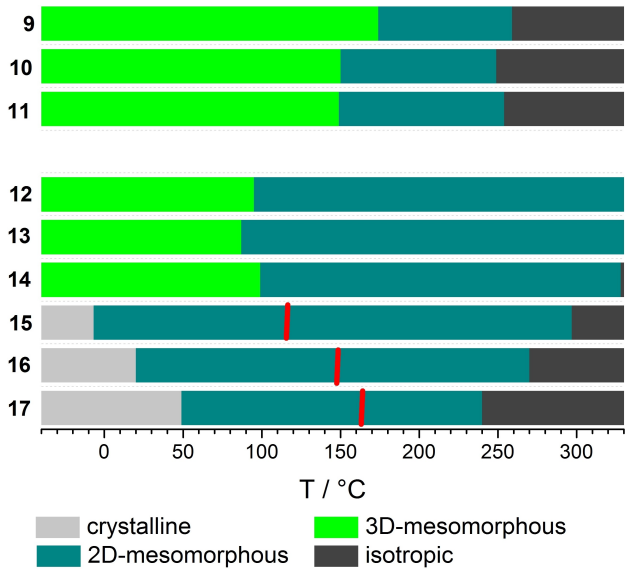

Figure 2. Phase widths (determined by DSC, 10 K/min, except **15**: 5 K/min; red line: a DSC-transition without change in XRD or POM).

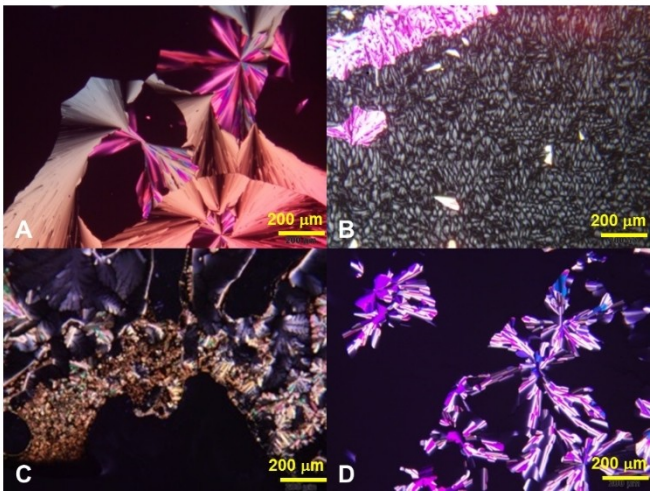

Figure 3. POM textures: (A) **9**, 220 °C, cooling 5 K/min, crossed polarizers; (B) **11**, 200 °C, cooling 5 K/min, 60° rotated polarizers; (C) **14**, 250 °C, cooling 5 K/min, decomposition, crossed polarizers; (D) **16**, 250 °C, cooling 1 K/min, crossed polarizers.

5 kJ mol^{-1}) can be correlated with negligible structural rearrangement at the transition to the liquid crystal, thus the structure is rather a highly organized mesophase than a soft crystal. This is in agreement with the XRD pattern, which has too few reflections for a soft crystal at low temperature. Furthermore, due to additional reflections (see Table 3), XRD analysis confirmed 3D structures for **9**–**14**.

The transition to the higher-ordered mesophase of 3,4-disubstituted derivatives **9**–**11** can also be observed with POM (Figure 3B, SI). Upon cooling below these transition temperatures, the 'black' areas of the homeotropic aligned columnar liquid crystal changed to birefringent textures. These textures are thermally reversible, they vanish on heating (190 °C) and rebuild on cooling (140 °C). However, the 3,4,5-tris-long chain derivatives **12**–**17** do not show this transition in POM, only loss of shearability was observed. On further cooling to room temperature, the film solidifies while retaining the texture. At 200 °C, samples of OXD-BTTs can be sheared easily but the viscosity increase with decreasing temperature. This impedes shearing below 95 °C for **12**–**14** or 150 °C for **15**–**17**. Similarly,

Table 3. **11**, **12** and **16** reflections, miller indices, π-π-distance, alkyl chain distance (halo), correlation length (ξ) and parameters (comparison of theoretical and experimental signals are given in the supporting information).[a]

	2θ (hk) [°]							π-π (halo) [Å]	ξ [π-π-distance]	Parameter [Å]	
11 (180 °C)	2.56 (10)		4.44 (11)	5.14 (20)	6.71 (21)				3.6 (4.5)	8	a_{hex} = 39.9
11 (130 °C)	2.33 (10)	2.65 (01)		4.59 (20)	5.30 (21;02)	7.00 (22)			3.5 (4.7)	16	a_{rec} = 38.5; b_{rec} = 33.5
11 (25 °C)	2.39 (10)	2.71 (01)	3.60 (11)	4.71 (20)	5.42 (21;02)	7.18 (22)	8.15 (03)		3.5 (4.5)	25	a_{or} = 37.6; b_{or} = 32.7
12 (210 °C)		3.24 (02)		6.05 (20)	8.58 (15)				3.5 (4.7)	13	a_{rec} = 30.0; b_{rec} = 54.6
12 (140 °C)	2.88 (10)	3.24 (11,02)	4.30 (12)	5.95 (21)	8.58 (15;24;31)				3.5 (4.4)	16	a_{rec} = 30.7; b_{rec} = 54.6
12 (70 °C)	2.80 (10)	3.23 (11;02)	4.27 (12)	5.60 (13;20)	7.03 (14)	7.40 (23)	8.52 (15;24;31)	9.78 (32)	3.5 (4.4)	26	a_{or} = 31.6; b_{or} = 54.8
12 (25 °C)	2.81 (10)	3.24 (11;02)	4.30 (12)	5.64 (13;20)	7.08 (14)	7.46 (23)	8.59 (15;24;31)	9.83 (32)	3.5 (4.3)	30	a_{or} = 31.4; b_{or} = 54.5
16 (205 °C)	2.58 (10)		4.41 (11)	5.13 (20)	6.74 (21)				3.6 (4.9)	14	a_{hex} = 39.6
16 (170 °C)	2.57 (10)		4.41 (11)	5.14 (20)	6.75 (21)	7.65 (30)		9.16 (31)	3.6 (4.9)	15	a_{hex} = 39.6
16 (135 °C)	2.58 (10)		4.42 (11)	5.13 (20)	6.75 (21)	7.65 (30)	8.84 (22)	9.18 (31)	3.5 (4.8)	17	a_{hex} = 39.6
16 (25 °C)	2.50 (10)		4.31 (11)	4.99 (20)					3.5 (4.6)	10	a_{hex} = 40.9

[a] hex: hexagonal, or: orthorhombic, rec: rectangular.

These are not the final page numbers! ↗↗

loss of shearability is observed for **9**–**11** below 155 °C. Anyway, the columnar order is substantiated by POM and XRD. Both groups form pseudo-focal-conical textures and show dendritic growth upon cooling from the isotropic phase, typically found[22] for columnar arrangement in liquid crystalline phases. The long-chain 3,4,5-trisubstituted derivatives (**16**, **17**) show mosaic textures already upon heating under the polarization microscope (SI). Uniquely, *N,N,N*-(trisdodecyloxyphenyl)benzo [1,2-*b*:3,4-*b*′:5,6-*b*′′]trithiophene-tricarboxamide,[3a] the only known analogue to the oxadiazole-derivative **15**, displays very similar thermal properties. Though an electron deficient 1,3,4-oxadiazole is replaced by a shorter carboxamide, clearing point (T_i = 285 °C) and melting point (T_m = −9 °C) are in the same temperature range.

Via temperature-dependent X-ray scattering on oriented fibers, the mesophase structure has been studied in detail for the representative compounds **11**, **12** and **16**. Oriented fibers were obtained by extrusion after 30 min annealing of the materials in the LC phase (**11**: 210 °C, **12**: 180 °C, **16**: 210 °C).

All diffraction patterns (Figure 4, Figure 6, Figure 7 and SI) show a signal in the wide angle range at the meridian which can be assigned to the π-π distances, a halo which corresponds to the liquid aliphatic chains, and on the equator a series of reflections indicating a 2D-positional order of the columns. The equatorial reflections can either be assigned to a hexagonal or a rectangular 2D grid. The lattice parameter varies complexly with temperature differences, due to structural changes (discussion see "**11**, **12**, **16** in more detail"). Hence, all results from POM, DSC and XRD are consistent with columnar mesophases.

The intracolumnar π-π-distances (Table 3) are calculated to be 3.5 Å–3.6 Å and the correlation length is estimated from the FWHM (Scherrer equation[23]) and is in agreement with 8–13 correlated molecules in the high temperature phase of **11**, **12** and **16**. Their correlation lengths are typical for liquid crystalline materials, which results from van-der-Waals, dipole and π-π interactions. As the mobility is higher in the high temperature phase, the correlation length is smaller, due to the enhanced liquid character of the material. With decreasing temperature a transformation to a 3D lattice occurs, the correlation length increases (Table 3) up to 30 molecules per column. At low temperature the correlation length is high, so that the phase can be characterized as a highly ordered mesophase. These high correlation lengths demonstrate the strong aromatic interactions in the 3D-ordered liquid crystal. Furthermore, the π-π distances decrease minimally for compound **11**, **12**, **16** with decreasing temperature.

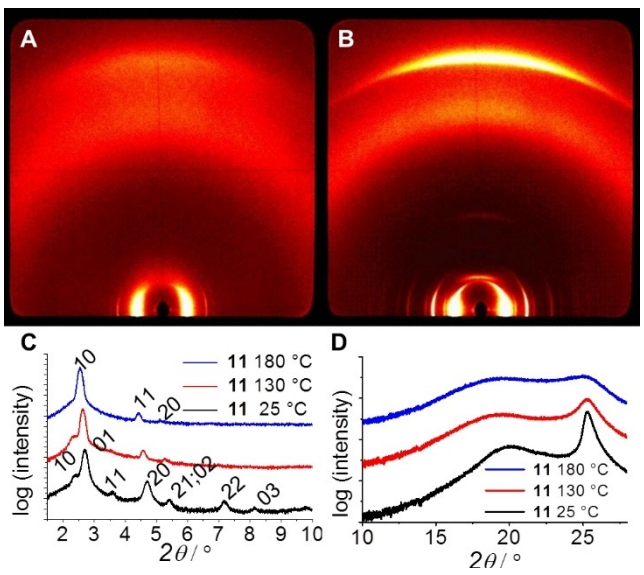

Figure 4. WAXs diffraction pattern of **11** at (A) 180 °C (B) 25 °C and corresponding plots (C), (E).

XRD-analysis of 11

Figure 4 shows the 2D X-ray patterns of compound **11** at 180 °C and 25 °C in the cooling process.

The equatorial reflections of **11** at 180 °C can be assigned to a hexagonal lattice (a_{hex} = 39.9 Å, Table 3). Upon cooling to 130 °C, additional reflections appear in the diffraction pattern (SI). This diffraction pattern also occurs at 25 °C, the reflections are here even more pronounced. The seven small angle reflections can be attributed to a primitive rectangular lattice with a = 37.7 Å and b = 32.8 Å at 25 °C. The structural reorientation (A) from hexagonal (B) to simple rectangular (C) is shown schematically in Figure 5. The tilts (color gradient) of the columns result in elliptical cross sections of the columns. For optimal space filling the columns are forced to shift (red arrow (A)), which finally leads to a rectangular unit cell.

Three further diffuse signals appear on the meridian at room temperature at certain layer lines L (Figure 4B, Figure 4D). These signals correspond to distances of d = 28.9 Å (L = 1), d = 14.4 Å (L = 2) and d = 9.5 Å (L = 3), thus a 3D-order of an orthorhombic lattice. This large periodicity and the rather diffuse character of the signals indicate a low correlation length along the columnar axes. Such periodicities are naturally achieved by helical stacking of star-shaped mesogens.[23]

XRD-analysis of 12

Figure 6 shows the XRD patterns upon cooling of **12**. The equatorial reflections can be assigned to a primitive rectangular lattice over the whole temperature range. At 140 °C and 210 °C

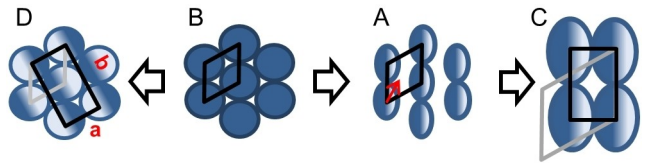

Figure 5. The hexagonal structure (B) rearranges via (A) to a simple rectangular cell (C). Tilting of the discs leads to an ellipsoid cross-section and shift of columns. Color gradient and red arrow illustrate tilt and shift direction. With different tilt directions, a centered rectangular cell (D) is formed. A,b: cell parameters of the rectangular lattice.

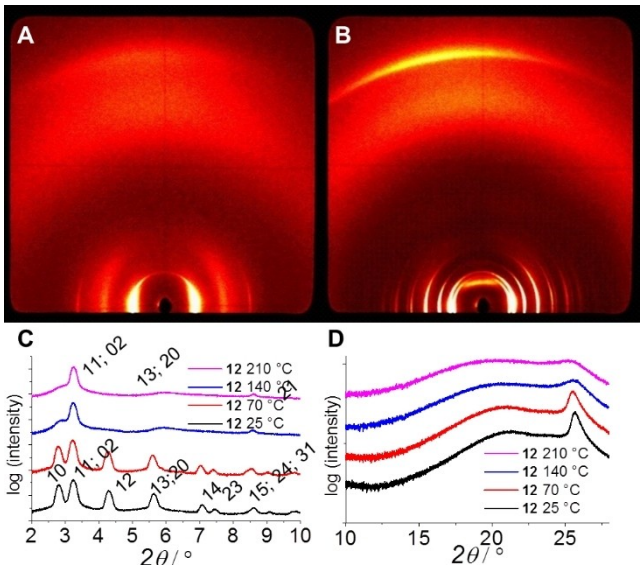

Figure 6. Diffraction patterns of **12** A) 210 °C, B) 70 °C, and corresponding plots C), D).

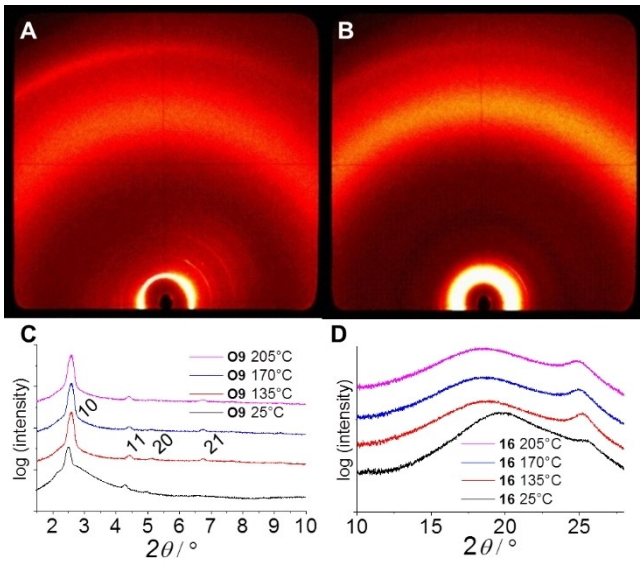

Figure 7. Diffraction pattern of 16 at A) 135 °C, B) 25 °C.

some reflections (01, 11, 20) are more diffuse and thus the 2D positional order is reduced in contrast to the pattern at lower temperature. Since the reflections become more diffuse or disappear here, it is possible that the rectangular phase changes at higher temperatures into a hexagonal lattice, which was not completed in the time frame of the X-ray measurement due to the low mobility at high viscosity. The sharper signals at 210 °C can then be assigned to the 10 and 21 reflections of a hexagonal lattice (a_{hex} = 31.5 Å). (See SI for comparison of theoretical and experimental signals).

Furthermore, the (0k = 2n + 1)-signals of the rectangular lattice are erased, due to a glide reflection along b. Figure 5 shows the hypothetical restructuring from a hexagonal to a rectangular centered grid. By tilting (color gradient) the central column oppositely to the edge columns the symmetry decreases. Thus, instead of two glide reflections along both axis (centered rectangular cell), just the one along b remains.

At lower temperatures, further diffuse reflections appear on the meridian, which correspond to the 001 signal (70 °C: 2θ = 2.17°, d = 40.7 Å; 25 °C: 2θ = 2.24°, d = 39.5 Å) and consequently, to a periodicity along the columns. Thus, below 70 °C, a change into a 3D correlated structure occurs (orthorhombic lattice, 70 °C: a_{or} = 31.6 Å, b_{or} = 54.8 Å). Also, the wide-angle signal, associated with the π-π distance, becomes more intense, but the intercolumnar spacing does not change significantly with decreasing temperature.

XRD-analysis of 16

Figure 7 shows the diffraction patterns obtained during the cooling process. While the diffraction patterns at 135 °C, 170 °C and 205 °C can be assigned to a hexagonal columnar mesophase (Table 3), the clear hexagonal diffraction pattern is lost at room temperature and a ring pattern indicates a reduced orientation.

At 205 °C **16** forms a hexagonal lattice (a_{hex} = 39.6 Å, Table 3) with π-π spacing of 3.6 Å. At 170 °C the diffraction pattern exhibits identical parameters but with decreasing temperature to 135 °C, an intensification of the meridional (π-π) and equatorial reflexes occurs, due to better intra- and intercolumnar order.

Cooling to the crystallization temperature range (T_m = 20 °C–36 °C) results in a reduction of order and forms a disordered soft crystal, crystallization of the alkyl chains is clearly visible by the more intense halo at 25 °C (Figure 7B). The intracolumnar correlation length of the columns decreases to ξ = 35.2 Å (11 molecules) and the π-π distance is slightly reduced to 3.5 Å.

In the heating curves of the long chain derivatives (**15**–**17**), low-enthalpy transitions (ca. 150 °C–170 °C) are also observed (Figures S4.7–S4.9 SI). In accordance with missing changes in the POM observations and the temperature independent structure of the mesophase (X-ray diffraction from 135 °C to 205 °C) this transition cannot undoubtedly correspond to a transition between mesophases with e.g. a weak helical order which is not detectable via XDR experiments. It can also be caused by partially crystalline regions Eichhorns *N,N′,N″*-(trisdodecyloxyphenyl)benzo[1,2-b:3,4-*b*′:5,6-*b*″]trithiophene-tricarboxamide[3a] exhibits a helical-columnar order in the hexagonal 2D-structure in the mesophase. Structural rearrangements at moderate temperatures were not observed for this amide, but the π-π-signal intensifies significantly between 80 °C and 70 °C. The major difference between this amide and BTT-OXDs is in the variation of the *a*-parameter by temperature. At 250 °C *a*(amide) = 37.5 Å and decreases upon cooling to *a*-(−25 °C) = 33.9 Å, while *a*(16) appears to be temperature-independent. This deviant behavior is attributed to the main the structural difference, the intermolecular H-bridges of the

amide. On the other hand, with increasing temperature the distance of the aromatic units decreases for the amide and 16.

Optical Properties

The following section describes the influences of polarity and concentration on the optical spectra in solution and the optical properties of pure substance films of the oxadiazole derivatives, the data are collected in Table 4.

11 (3,4-OC14, SI) and **12** (3,4,5-OC6) were investigated as representatives for this substance class with respect to their optical and solvatochromic properties. **8** (4-OC3) could not be investigated because of its low solubility. The investigation of other homologous compounds was omitted, since the alkyl chain length in the dissolved state has no influence on the position and shape of the absorption and emission spectra. However, the lipophilicity of the periphery influences the aggregation of the chromophores in poor solvents. To illustrate the aggregation behavior as a function of the number of chains, representatives with identical chain length, **11** with 3,4-ditetradecyl- and **16** with 3,4,5-tritetradecyl-substitution, were examined in systematically varied solvent mixtures (Figures S9.1–S9.3, SI).

For the measurement of solvatochromism, a millimolar solution in dichloromethane was diluted to 10 μM for the absorption measurements and to 0.1 μM for the fluorescence measurements. The aggregation behavior in absorption and emission was investigated in 10 μM solvent mixtures of THF/heptane or THF/water. Fluorescence quantum yields were determined via the ratios of the integrated emission bands of the compound and of a 0.2 μM quinine sulfate solution in 0.1 M sulfuric acid.[25]

The absorption spectra of 3,4-di- and 3,4,5-tri-alkoxy substituted OXD-BTTs **11**, **12** are very similar but the third alkoxy chain shifts the emission to the red. Solvatochromism in good solvents is negative but small (toluene–dichloromethane: $\Delta\lambda \leq -4$ nm) (Table 4, Figure 8). These marginal shifts correlate with DFT calculations, since electronic transitions between the highest three occupied and the lowest three unoccupied orbitals do not significantly change the spatial charge distribution (SI). Poor solvents provoke stronger effects, but these are attributed to aggregation. In polar solvents (acetone, MeOH, DMSO, acetonitrile), the investigated OXD-BTT show a decrease in absorbance, broadening of the absorption bands and an increase of the baselines at higher wavelengths. The latter is mainly caused by aggregation of the nonpolar fluorophores and light scattering at the aggregates. Figure 8 shows the influence of aggregation on the absorption by comparison of spectra from 10^{-5} M and 10^{-6} M solution of **12** in acetone and acetonitrile.

Whereas the 10 μM solutions of **12** in both solvents result in largely broadened absorption bands, dilution to 1 μM gives a typical absorption band with a sharp long-wave edge in acetone but the 1 μM concentration in the more polar acetonitrile has no influence on the shape of the absorption band. In the non-polar but also poor solvent cyclohexane, the main absorption bands are slightly broadened, this is more pronounced for **11** (SI) than for **12**. In addition, the vibrational fine structure is blurred in the polar solvents. A closer look at the individual spectra shows that up to three main or secondary maxima can be assigned to each graph. These maxima occur at a distance of about 20 nm from each other and correspond to different vibration modes. The spectra and position of main and side maxima are collected in the supporting information.

The 3,4- and the 3,4,5-derivatives (**11**,**12**) also show vibrational structures in the emission bands (Figure 9) in non-polar solvents and an attenuation of the fluorescence in polar solvents. If the polarizability of the solvent is increased by replacing cyclohexane with toluene or benzene, the fluorescence quantum yield increases to 18% (toluene) and 30% (benzene) (Table 4). The hyperchromic effect in good solvents is more likely to be understood as a result of better

Table 4. Optical properties of **11** and **12**.[a]

Solvent	**11** λ^{A}_{max} [nm]	logε_{max}	λ^{F}_{max} [nm]	$\tilde{\nu}_{stokes}$[cm^{-1}]	QY [%]
CH	358	4.76	410	3543	15
T	358	5.03	416	3895	16
DCM	356	5.06	418	4166	21
AT	346	4.87	444	6379	7
ACN	348	4.83	457	6854	2
Film			454		
Film temp.			467		
Solvent	**12** λ^{A}_{max} [nm]	logε_{max}	λ^{F}_{max} [nm]	$\tilde{\nu}_{stokes}$[cm^{-1}]	QY [%]
CH	346	4.94	415	4805	8
T	356	5.03	417	4109	18
DCM	352	5.07	445	5937	31
AT	346	4.74	465	7396	12
ACN	366	4.64	464	5771	6
Film			459		
Film temp.			460		

[a] CH: cyclohexane, T: toluene, DCM: dichloromethane, AT: acetone, ACN: acetonitrile.

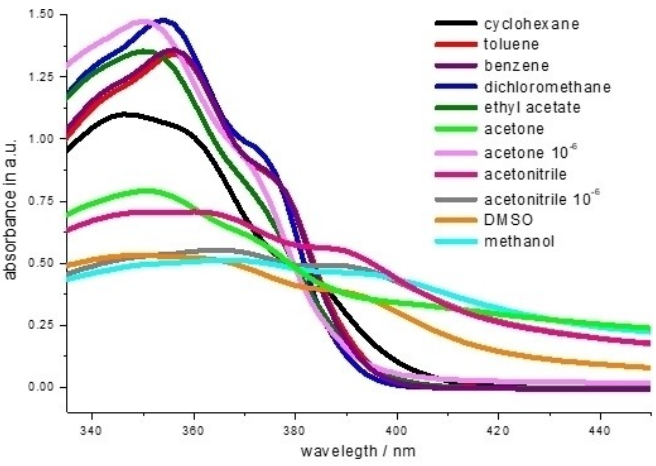

Figure 8. UV-vis spectra of **12** (the 10^{-6} M solution was studied in a 5-cm-cuvette and corrected to same path length).

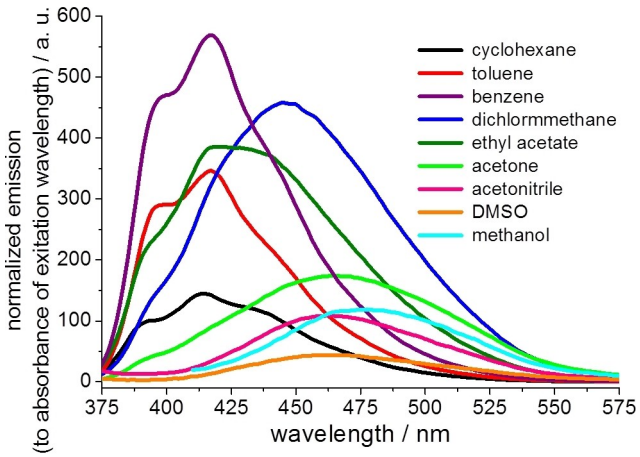

Figure 9. Emission spectra of **12**: normalized to the absorption at the excitation wavelength.

molecular solvation while in poor solvents, aggregates form. Dichloromethane and benzene are good solvents, the fluorescence quantum yields reach 30% whereas in poor solvents like methanol or cyclohexane aggregates are formed and the quantum yields are reduced to about 7%.

The fluorescence of OXD-BTTs in highly polar solvents (acetone, acetonitrile, methanol, DMSO) is severely shifted to lower energies. The red-shift and reduced quantum yields are attributed to aggregation since the emission of films of these compounds and their solutions in polar solvents have similar characteristics, the maxima of films and solution spectra (SI) are almost identical. Like emission, the HOMO-LUMO gap is influenced by aggregation. Determined from the absorption edge, the band gap of **11**, **12** is $\Delta E = 3.1$ eV ($\lambda = 404$ nm) in a good solvent like THF.

As aggregation has a decisive influence on position, shape and intensity of absorption and emission spectra, we examined the behavior of OXD-BTTs **11**, **16** (3,4-di- and 3,4,5-tritetradecyl-derivatives) in THF-solvent mixtures with increasing amounts of water or heptane as poor solvents (SI).

A decreasing solvent quality provokes increasing aggregation. This reduces the absorbance of **11**, **16** and a shoulder in the longer wavelength range appears (water: **11**: 388; **16**: 387). The position of the shoulder can be brought into agreement with the maxima observed in the solvatochromism measurements, which belong to the absorption of aggregates. Increasing heptane concentration results in an attenuation of the emission, in THF/heptane 10/90, only 32% of integral emission of **11** in pure THF is left, in THF/water mixtures, the decay is even more drastic. From THF/heptane 10/90, only 6% of the intensity from **11** in THF was detected. The behavior of **16** in THF/heptane is identical but the sensitivity to water is much lower, the integral emission of **16** in 90% water is only reduced to 32%.

Solvatochromism and aggregation study reveal that the triple-substituted OXD-BBTs **12**, **16** are stronger fluorophores with less impact of aggregation on the emission.

Conclusion

Threefold Huisgen reaction affords OXD-BTTs in moderate to good yields. Except **8**, all synthesized compounds are thermotropic liquid crystals and show characteristic textures (POM) and broad mesophases ($\Delta T \geq 289$ K). The phase width and mesophase structure are strongly related to the substitution pattern of the attached alkoxy phenyl rings.

DSC of the three groups of DLCs (**9**–**11**, **12**–**14**, **15**–**17**) show meso-meso-transitions, these are also visible in POM and XRD for **9**–**11**, but not in POM for **12**–**14**. Contrary to DSC, neither POM nor XRD show these transitions for **15**–**17**, but these are the only compounds which show crystallization.

The 3,4-dialkoxy derivatives undergo a structural reorientation between a high temperature hexagonal phase and a rectangular low temperature mesophase. Similarly, the short chain 3,4,5-trialkoxy DLCs exhibit two mesophases. DSC of the long-chain 3,4,5-compounds shows in a clear crystallization signal, and the structure of the mesophase (XRD, POM) is consistent over the whole LC range. DSC shows a further transition at about 150–170 °C, which could be related to a meso-meso transition with weak structural change (e.g. a weak helical structure). All investigated compounds show strong π-π-interactions (3.5–3.6 Å) and a good columnar orientation. For the rectangular phases even a weak 3D-order along the columns was found.

In general, the 3,4,5-trisubstituted derivatives **14**–**16** have larger phase widths in the 2D mesophase and higher clearing points than their 3,4-disubstituted analogues **9**–**11** (Table 2, Figure 2). The shorter-chain OXD-BTTs (**12**–**14**) have wider phase widths of the 2D mesophase than their higher homologues (**15**–**17**). OXD-BTTs are slightly yellow compounds which emit blue light. In good solvents the fluorescence quantum yields reach 30%. Aggregation quenches the fluorescence and shifts the maximum to the red.

Experimental Section

Experimental Details

^{1}H and ^{13}C NMR spectra: Bruker Avance III HD 300 (300 MHz, 75 MHz), Bruker Avance II 400 (400 MHz, 101 MHz), and Bruker Avance III 600 (600 MHz, 151 MHz), solvents were $CDCl_3$, C_6D_6, DMSO-d_6. Chemical shifts are expressed as δ values in ppm, coupling constants are given in Hz. Calibration on the residual ^{1}H signal of the solvent, in $CDCl_3$/DMSO mixtures calibration on DMSO. Assignments of ^{1}H and ^{13}C signals on the basis of HSQC and HMBC experiments. Abbreviations used for assignment of spectra: ph: phenyl, tet: tetrazole, oxa: 1,3,4-oxadiazole, BTT: benzotrithiophene. Melting points: Büchi HWS SG 200, Stuart Scientific SMP3. IR: JASCO 4100 FT-IR (ATR), FD-MS: Mat 95 (Finnigan); HR-ESI: Q-TOF-ULTIMA 3, Lock Spray device (Waters-Micromass), NaICsI as reference. UV-vis: Perkin-Elmer Lambda 16. Fluorescence: Perkin-Elmer LS 50B; Photochemistry: LOT Xe-arc lamp, 300 W, equipped with IR-filter and color filters. Polarized microscopy: Olympus BX51, ColorView Olympus camera, heattable Linkam LTS 350 for temperature regulation. DSC: Perkin Elmer DSC7, heating rate: 10 K min^{-1}. Details for synthesis of intermediates are collected in the SI. 2D-X-Ray Analysis: The temperature-dependent middle angle X-ray scattering

MAXS (sample-detector distance 28 cm; $2\theta max = 11.5°$) and wide angle X-ray scattering WAXS (sample-detector distance 13 cm; $2\theta max = 25°$ or with by 14° tilted detector, sample-detector distance 21 cm, $2\theta max = 28.5°$) investigations were performed on a Bruker Nanostar (Detector Vantec2000, Microfocus copper anode X-ray tube Incoatec). The samples were prepared by fibre extrusion using a mini-extruder. The mini-extruder consisted of a cylindrical stainless-steel container of 2 mm diameter with a nozzle of 0.7 mm diameter. The container was heated to the temperature range of the liquid crystal and the fibre was extruded manually via the nozzle with a cylindrical steel pistil. The measurements were carried out in Mark capillaries (Hilgenberg) positioned perpendicular to the incident X-ray beam. All X-ray data was processed and evaluated with the program datasqueeze (http://www.datasqueezesoftware.com/) Silver behenate was used as calibration standard for MAXS and WAXS studies.

2,5,8-Tris(5-(4-propyloxyphenyl)-1,3,4-oxadiazol-2-yl)benzo [1,2-b:3,4-b′:5,6-b″]trithiophene 8

Under nitrogen atmosphere, 84.4 mg (0.22 mmol, 1.0 eq.) benzo [1,2-b;3,4-b′;5,6-b″]trithiophene-2,5,8-tricarboxylic acid and 4 mL thionyl chloride were heated to 80 °C for 60 h. The obtained benzo [1,2-b;3,4-b′;5,6-b″]trithiophene-2,5,8-tricarbonyl trichloride was freed from excess thionyl chloride by distillation at atmospheric pressure in the absence of moisture. The acid chloride was suspended under inert atmosphere in 10 mL absolute toluene and mixed with 169.9 mg (0.83 mmol, 3.8 eq.) of 5-(4-propyloxyphenyl)-*2H*-tetrazole and 0.2 mL (1.5 mmol, 6.8 eq.) of 2,4,6-collidine. The reaction mixture was stirred for 2 h at 60 °C and then at 80 °C for a further 17 h under nitrogen atmosphere. After cooling to room temperature, the solid was filtered off, washed with 2 N aq. hydrochloric acid, 2 N aq. sodium hydroxide and water. The dried residue was washed with dichloromethane. **Yield**: 0.105 g (0.12 mmol ≙ 55 %) of an off-white, yellowish solid with m.p. 323 °C (dec.). Single crystals were grown from hot 1,2-dichlorobenzene.

IR (ATR): $\tilde{\nu}$ [cm^{-1}] = 2963 w, 2935 w, 2871 w, 1609 m, 1590 m, 1492 s, 1470 m, 1307 m, 1272 m, 1257 ss, 1174 s, 1081 m, 1042 m, 1014 m, 833 m, 746 ss, 707 m.

2,5,8-Tris(5-(3,4-bis(decyloxy)phenyl)-1,3,4-oxadiazol-2-yl) benzo[1,2-b:3,4-b′:5,6-b″]trithiophene 9

Under nitrogen atmosphere, 71.1 mg (0.19 mmol, 1.0 eq.) of benzo [1,2-b;3,4-b′;5,6-b″]trithiophene-2,5,8-tricarboxylic acid were covered with 4 mL thionyl chloride and heated to 80 °C for 48 h. The obtained benzo[1,2-b;3,4-b′;5,6-b″]trithiophene-2,5,8-tricarbonyl trichloride was freed from excess thionyl chloride by distillation at atmospheric pressure in the absence of moisture. The acid chloride was suspended under nitrogen atmosphere in 10 mL absolute toluene and mixed with 284.2 mg (0.62 mmol, 3.3 eq.) 5-(3,4,-bis (decyloxy)phenyl)-*2H*-tetrazole and 0.1 mL (0.75 mmol, 3.9 eq.) 2,4,6-collidine. The reaction mixture was stirred for 24 h at 80 °C under nitrogen atmosphere. After cooling to room temperature 10 mL 2 N hydrochloric acid and 10 mL chloroform were added to the mixture. The organic phase was separated and the aqueous phase was extracted with chloroform (2×10 mL). The combined organic extracts were washed with brine, dried over magnesium sulfate and adsorbed on silica gel. The crude product was purified by column chromatography (SiO_2). In order to remove by-products, first pure toluene was used as eluent; afterwards the polarity of the mobile phase was gradually increased to a mixture of toluene and ethyl acetate (1:1). In order to separate further by-products, the resulted mixture was adsorbed on aluminum oxide (neutral) and the by-product eluted with ethyl acetate. The pure product was eluted with chloroform from the stationary phase to yield 89.2 mg (5.5 mmol ≙ 29 %) of a yellow solid.

^{1}H-NMR (400 MHz, $CDCl_3$): δ [ppm] = 7.62 (s, 1H, H3-BTT), 7.30 (dd, ^3J = 8.4 Hz, ^4J = 1.9 Hz, 1H, H6-ph), 7.20 (d, ^4J = 1.6 Hz 1H, H2-ph), 6.78 (d, ^3J = 8.5 Hz, 1H, H5-ph), 3.99 (t, ^3J = 6.7 Hz, 2H, OCH_2), 3.91 (t, ^3J = 6.6 Hz, 2H, OCH_2), 1.89–1.82 (m, 4H, CH2), 1.54–1.31 (m, 28H, CH_2), 0.93–0.89 (m, 9H, CH_3). **^{13}C-NMR (100 MHz, $CDCl_3$)**: δ [ppm] = 164.64, 159.28, 152.39, 149.18, 134.31, 130.70, 125.38, 122.67, 120.29, 115.06, 112.40, 110.78, 69.12, 69.05, 32.15, 32.13, 29.98, 29.91, 29.91, 29.86, 29.77, 29.63, 29.59, 29.56, 29.44, 26.36, 26.27, 22.89, 14.30. **IR (ATR)**: $\tilde{\nu}$ [cm^{-1}] = 2952 m, 2917 ss, 2849 s, 1609 m, 1590 w, 1498 ss, 1465 m, 1394 m, 1277 s, 1251 m, 1227 s, 1143 m, 1107 m, 1067 m, 1020 m, 986 m, 843 m, 806 m, 736 m, 722 m, 666 m. **MALDI-MS**: 1617.0 calculated for $C_{96}H_{138}N_6O_9S_3 + H^+$; found: 1616.8.

2,5,8-Tris(5-(3,4-bis(dodecyloxy)phenyl)-1,3,4-oxadiazol-2-yl) benzo[1,2-b:3,4-b′:5,6-b″]trithiophene 10

Following the procedure given for **9**„ 29.0 mg (0.077 mmol, 1.0 eq.) benzo[1,2-b;3,4-b′;5,6-b″]trithiophene-2,5,8-tricarboxylic and 150.2 mg (0.29 mmol, 3.8 eq.) 5-(3,4-bis(dodecyloxy)phenyl)-*2H*-tetrazole and 0.05 mL (0.38 mmol, 4.9 eq.) 2,4,6-collidine gave, after stirring 19 h at 80 °C, usual work-up, and column chromatography (SiO_2 (2×18 cm) pure toluene as first eluent, polarity of the mobile phase was gradually increased to a mixture of toluene and ethyl acetate (4:1)) to yield 95.9 mg (0.054 mmol ≙ 70 %) of a yellowish solid.

^{1}H-NMR (400 MHz, $CDCl_3$): δ [ppm] = δ 8.02 (s, 1H, H3-BTT), 7.55 (dd, ^3J = 8.3 Hz, ^4J = 2.0 Hz, 1H, H6-ph), 7.47 (d, ^4J = 2.0 Hz, 1H, H2-ph), 6.92 (d, ^3J = 8.5 Hz, 1H, H5-ph), 4.08–4.03 (m, 4H, OCH_2), 1.92–1.84 (m, 4H, CH_2), 1.56–1.48 (m, 4H, CH_2), 1.45–1.25 (m, 32H, CH_2), 0.91–0.88 (m, 6H, CH_3). **^{13}C-NMR (100 MHz, $CDCl_3$)**: δ [ppm] = 164.98, 159.72, 152.64, 149.41, 134.94, 131.19, 125.65, 123.39, 120.64, 115.42, 112.74, 111.34, 69.42, 69.21, 32.11, 29.95, 29.91, 29.89, 29.86, 29.76, 29.68, 29.57, 29.48, 29.36, 26.30, 26.23, 22.87, 14.29.

IR (ATR): $\tilde{\nu}$ [cm^{-1}] = 2960 m, 2920 ss, 2852 s, 1605 m, 1589 m, 1498 s, 1467 m, 1449 m, 1393 m, 1272 s, 1214 m, 1138 m, 999 m, 859 m, 830 m, 807 m, 720 m. **MALDI-MS**: 1785.2 calculated for $C_{108}H_{162}N_6O_9S_3 + H^+$; found: 1784.9.

2,5,8-Tris(5-(3,4-bis(tetradecyloxy) phenyl)-1,3,4-oxadiazol-2-yl)benzo[1,2-b:3,4-b′:5,6-b″] trithiophene 11

Following the procedure given for **9**, 37.8 mg (0.10 mmol, 1.0 eq.) benzo[1,2-b;3,4-b′;5,6-b″]trithiophene-2,5,8-tricarboxylic and 274.9 mg (0.482 mmol, 4.4 eq.) 5-(3,4-bis(tetradecyloxy)phenyl)-*2H*-tetrazole and 0.1 mL (0.75 mmol, 8.3 eq.) 2,4,6-collidine gave, after stirring 19 h at 80 °C, usual work-up, and column chromatography (SiO_2, toluene: ethyl acetate = 1:0, 40:1, 30:1, 10:1)) to yield 66.4 mg (34.0 μmol ≙ 34 %) of a yellowish solid.

^{1}H-NMR (300 MHz, $CDCl_3$): δ [ppm] = 8.11 (s, 1H, H3-BTT), 7.60 (dd, ^3J = 8.4 Hz, ^4J = 2.0 Hz, 1H, H6-h), 7.53 (d, ^4J = 2.0 Hz, 1H, H2-ph), 6.94 (d, ^3J = 8.4 Hz, 1H, H5-ph), 4.08 (t, ^3J = 6.6 Hz, 4H, OCH_2), 1.92–1.84 (m, 4H, CH_2), 1.54–1.47 (m, 4H, CH_2), 1.39–1.27 (m, 40H, CH_2), 0.91–0.85 (m, 6H, CH_3). **^{13}C-NMR (100 MHz, $CDCl_3$)**: δ [ppm] = 165.09, 159.87, 152.72, 149.49, 135.18, 131.37, 125.73, 123.66, 120.75, 115.56, 112.86, 111.54, 69.52, 69.26, 32.10, 29.92, 29.91, 29.87, 29.85, 29.84, 29.70, 29.64, 29.55, 29.44, 29.33, 26.27, 26.21, 22.86, 14.29. **IR (ATR)**: $\tilde{\nu}$ [cm^{-1}] = 2917 ss, 2850 ss, 1732 w, 1605 m, 1590 m, 1497 s, 1466 s, 1393 m, 1273 s, 1215 m, 1143 m, 1090 m,

1038 m, 1002 m, 858 m, 826 w, 804 m, 720 m, 653 m. **MALDI-MS**: 1953.4 calculated for $C_{120}H_{186}N_6O_9S_3+H^+$; found: 1953.3

2,5,8-Tris(5-(3,4,5-tris(hexyloxy)phenyl)-1,3,4-oxadiazol-2-yl) benzo[1,2-b:3,4-b′:5,6-b″]trithiophene (12)

According to the procedure given for **9**, 85.9 mg (0.23 mmol, 1.0 eq.) benzo[1,2-b;3,4-b′;5,6-b″]trithiophene-2,5,8-tricarboxylic and 356.8 mg (0.80 mmol, 3.5 eq.) 5-(3,4,5-tris(hexyloxy)phenyl)-*2H*-tetrazole and 0.1 mL (0.75 mmol, 3.3 eq.) 2,4,6-collidine gave, after stirring for 20 min at 60 °C 20 h at 80 °C, usual work-up, and column chromatography (SiO_2 (2.5×23 cm), Al_2O_3 (2.5×1.5 cm, toluene to toluene/ethyl acetate = 10:1). In order to remove further by-products the obtained mixture was dissolved in dichloromethane and the product precipitates by addition of ethyl acetate to yield 62.6 mg (0.18 mmol ≙ 80 %) of a pale yellow solid.

^{1}H-NMR (400 MHz, $CDCl_3$): δ [ppm] = 8.08 (s, 1H, H3-BTT), 7.20 (s, 2H, H2-ph,H6-ph), 4.09–4.03 (m, Hz, 6H, OCH_2), 1.92–1.75 (m, 6H, CH_2), 1.59–1.49 (m, 6H, CH_2), 1.43–1.34 (m, 12H, CH_2), 0.97–0.92 (m, 9H, CH_3). **^{13}C-NMR (100 MHz, $CDCl_3$)**: δ [ppm] = 165.07, 159.96, 153.72, 141.78, 135.04, 131.20, 125.63, 123.55, 117.65, 105.34, 73.72, 69.47, 31.95, 31.83, 30.54, 29.53, 26.00, 25.93, 22.87, 22.84, 14.26 (d, J = 2.2 Hz). **IR (ATR)**: $\tilde{\nu}$ [cm^{-1}] = 2956 s, 2927 s, 2871 m, 2857 m, 1587 s, 1547 m, 1488 ss, 1467 s, 1435 ss, 1379 m, 1348 s, 1321 m, 1240 s, 1214 s, 1112 ss, 1046 m, 1006 s, 909 m, 874 m, 839 s, 723 ss, 673 m. **MALDI-MS**: 1580.9 calculated for $C_{90}H_{126}N_6O_{12}S_3+H^+$; found: 1580.9.

2,5,8-Tris(5-(3,4,5-tris(octyloxy)phenyl)-1,3,4-oxadiazol-2-yl) benzo[1,2-b:3,4-b′:5,6-b″]trithiophene 13

According to the procedure given for **9**, 33.3 mg (88.0 μmol, 1.0 eq.) benzo[1,2-b;3,4-b′;5,6-b″]trithiophene-2,5,8-tricarboxylic and 159.2 mg (0.3 mmol, 3.4 eq.) 5-(3,4,5-tris(octyloxy)phenyl)-2H-tetrazole and 0.1 mL (0.75 mmol, 8.6 eq.) 2,4,6-collidine gave, after stirring for 24 h at 80 °C, and usual work-up a crude product that was dissolved in dichloromethane and adsorbed on neutral aluminium oxide. The crude product was obtained by column chromatography (neutral $_{Al2O3}$ (1×3 cm)). In order to remove by-products pure ethyl acetate was used as eluent and the product was eluted with 10 % methanol in dichloromethane. In order to remove remaining by-products the obtained mixture was dissolved in dichloromethane and the product precipitates by addition of ethyl acetate. Yield: 43.3 mg (23.6 μmol ≙ 27 %) of an off-white solid

^{1}H-NMR (300 MHz, CDCl3): δ [ppm] = 8.24 (s, 1H, H3-BTT), 7.30 (s, 2H, H2-ph, H6-ph), 4.13-4.05 (m, 6H, OCH_2), 1.94-1.75 (m, 6H, CH_2), 1.58–1.25 (m, 30H, CH_2), 0.93–0.88 (m, 9H, CH_3). **^{13}C-NMR (100 MHz, CDCl3)**: δ [ppm] = 165.14, 160.02, 153.76, 141.85, 135.13, 131.30, 125.68, 123.70, 117.72, 105.45, 73.76, 69.52, 32.11, 32.05, 30.60, 29.75, 29.64, 29.59, 29.52, 26.36, 26.29, 22.87, 14.29. **IR (ATR):** $\tilde{\nu}$ [cm^{-1}] = 2960 s, 2919 ss, 2851 s, 1697 w, 1587 s, 1547 m, 1490 s, 1467 s, 1437 s, 1383 m, 1348 m, 1321 m, 1239 m, 1216 s, 1115 ss, 1008 s, 965 w, 838 m, 772 s, 743 w, 724 s, 626 w. **MALDI-MS**: 1833.2 calculated for $C_{108}H_{162}N_6O_{12}S_3+H^+$; found: 1832.9.

2,5,8-Tris(5-(3,4,5-tris(decyloxy)phenyl)-1,3,4-oxadiazol-2-yl) benzo[1,2-b:3,4-b′:5,6-b″]trithiophene 14

Following the procedure given for **9**, 35.1 mg (92.6 μmol, 1.0 eq.) benzo[1,2-b;3,4-b′;5,6-b″]trithiophene-2,5,8-tricarboxylic and 193.96 mg (0.3 mmol, 3.4 eq.) 5-(3,4,5-tris(decyloxy)phenyl)-2H-tetrazole and 0.1 mL (0.75 mmol, 8.1 eq.) 2,4,6-collidine gave, after stirring 24 h at 80 °C, usual work-up, a crude material. This was purified by column chromatography (Al_2O_3 (neutral) 1×3 cm). In order to remove by-products pure ethyl acetate was first used as eluent before the product was finally eluted from the stationary phase with 10 % methanol in dichloromethane. The residue was dissolved in dichloromethane and pure product was precipitated by addition of acetone. and column chromatography (SiO_2, toluene: ethyl acetate = 1:0, 40:1, 30:1, 10:1)) to yield 46.4 mg (22.3 μmol ≙ 24 %) of a yellowish solid.

^{1}H-NMR (400 MHz, $CDCl_3$): δ [ppm] = 8.22 (s, 1H, H3-BTT), 7.28 (s, 2H, H2-ph, H6-ph), 4.11 (t, ^3J = 6.4 Hz, 4H, OCH_2), 4.06 (t, ^3J = 6.5 Hz, 2H, OCH_2), 1.93–1.86 (m, 6H, CH_2), 1.57–1.48 (m, 6H, CH_2), 1.42–1.25 (m, 36H, CH_2), 0.91–0.87 (m, 9H, CH_3). **^{13}C-NMR (100 MHz, $CDCl_3$)**: δ [ppm] = 165.19 (C5-oxa), 160.10 (C2-oxa), 153.79 (C3-ph, C5-ph), 141.84 (C4-ph), 135.28 (C-BTT), 131.39 (C-BTT), 125.70 (C-BTT), 123.82 (C2-BTT), 117.79 (C1-ph), 105.49 (C2-ph, C6-ph), 73.78 (OCH_2), 69.53 (OCH_2), 32.13, 32.10, 30.58, 29.95, 29.87, 29.82, 29.80, 29.67, 29.59, 29.57, 26.35, 26.29, 22.87, 14.29 (CH_3). **IR (ATR)**: $\tilde{\nu}$ [cm^{-1}] = 2921 ss, 2852 s, 1587 m, 1547 m, 1490 s, 1467 s, 1437 s, 1380 m, 1348 m, 1321 w, 1239 m, 1214 m, 1116 s, 1007 m, 838 m, 723 s, 619 w. **MALDI-MS**: 2085.4 calculated for $C_{126}H_{198}N_6O_{12}S_3+H^+$; found: 2085.2.

2,5,8-Tris(5-(3,4,5-tris(dodecyloxy) phenyl)-1,3,4-oxadiazol-2-yl)benzo[1,2-b:3,4-b′:5,6-b″] trithiophene 15

Following the procedure given for **9**, 34.9 mg (0.092 mmol, 1.0 eq.) benzo[1,2-b;3,4-b′;5,6-b″]trithiophene-2,5,8-tricarboxylic and 227.8 mg (0.33 mmol, 3.7 eq.) 5-(3,4,5-tris(dodecyloxy)phenyl)-2H-tetrazole and 0.1 mL (0.75 mmol, 8.3 eq.) 2,4,6-collidine gave, after stirring 20 h at 80 °C, usual work-up, a crude material. This was purified by column chromatography (Al_2O_3 (neutral) topped with bas. Al_2O_3). In order to remove by-products pure ethyl acetate was first used as eluent before the pure product was eluted from the stationary phase with chloroform to yield 0.127 g (0.054 mmol ≙ 59 %) of a pale yellow solid with m. p. = −7 °C (onset, DSC).

^{1}H-NMR (300 MHz, $CDCl_3$): δ [ppm] = 8.14 (s, 1H, H3-BTT), 7.24 (s, 2H, H2-ph, H6-ph), 4.11–4.04 (m, 6H, OCH_2), 1.94–1.74 (m, 6H, CH_2), 1.58–1.50 (m, 6H, CH_2), 1.44–1.26 (m, 48H, CH_2), 0.91–0.85 (m, 9H, CH_3). **^{13}C-NMR (75 MHz, $CDCl_3$)**: δ [ppm] = 165.15, 160.02, 153.76, 141.82, 135.14, 131.30, 125.68, 123.67, 117.71, 105.43, 73.75, 69.50, 32.11, 30.61, 29.96, 29.93, 29.90, 29.83, 29.71, 29.58, 29.57, 26.37, 26.32, 22.86, 14.28. **IR (ATR)**: $\tilde{\nu}$ [cm^{-1}] = 2951 m, 2920 ss, 2851 ss, 1588 s, 1547 m, 1490 s, 1466 s, 1437 s, 1379 m, 1348 s, 1321 m, 1239 m, 1214 m, 1116 ss, 1051 m, 1006 s, 966 m, 838 m, 723 s. **MALDI-MS**: 2445.6 calculated for $C_{144}H_{234}N_6O_{12}S_3+Ag^+$; found: 2445.5.

2,5,8-Tris(5-(3,4,5-tris(tetradecyloxy) phenyl)-1,3,4-oxadiazol-2-yl)benzo[1,2-b:3,4-b′:5,6-b″] trithiophene 16

According to the procedure given for **9**, 34.6 mg (91.4 μmol, 1.0 eq.) benzo[1,2-b;3,4-b′;5,6-b″]trithiophene-2,5,8-tricarboxylic and 233.4 mg (0.30 mmol, 3.0 eq.) 5-(3,4,5-tris(tetradecyloxy)phenyl)-2H-tetrazole and 0.1 mL (0.75 mmol, 8.3 eq.) 2,4,6-collidine gave, after stirring for 18 h at 80 °C, and usual work-up a crude product. This was purified by column chromatography (Al_2O_3 (neutral)) topped with bas. Al_2O_3). In order to remove by-products, pure ethyl acetate was first used as eluent before the product was finally eluted from the stationary phase with chloroform. The residue was dissolved in chloroform and the pure product was precipitated by addition of acetone to yield 80.5 mg (31.1 μmol ≙ 34 %) of a slightly yellow solid with m. p. = 20 °C (onset, DSC).

^{1}H-NMR (300 MHz, $CDCl_3$): δ [ppm] = 8.25 (s, 1H, H3-BTT), 7.31 (s, 2H, H2-ph, H6-ph), 4.13–4.05 (m, 6H, OCH_2), 1.94–1.75 (m, 6H, CH_2), 1.60–1.50 (m, 6H, CH_2), 1.40–1.26 (m, 60H, CH_2), 0.90–0.85 (m, 9H, CH_3). **^{13}C-NMR (75 MHz, $CDCl_3$):** δ [ppm] = 165.22, 160.14, 153.81, 141.88, 135.35, 131.44, 125.72, 117.84, 105.57, 73.81, 69.56, 32.10, 30.58, 29.95, 29.92, 29.87, 29.80, 29.67, 29.55, 26.35, 26.29, 22.86, 14.28. **IR (ATR):** $\tilde{\nu}$ [cm^{-1}] = 2951 m, 2920 ss, 2851 ss, 1588 m, 1547 m, 1490 s, 1466 s, 1438 s, 1379 m, 1348 m, 1320 m, 1240 m, 1214 m, 1118 ss, 1045 m, 1008 s, 970 m, 839 m, 808 m, 723 ss. **MALDI-MS**: 2591.0 calculated for $C_{162}H_{271}N_6O_{12}S_3 + H^+$; found: 2591.0.

2,5,8-Tris(5-(3,4,5-tris(hexadecyloxy) phenyl)-1,3,4-oxadiazol-2-yl)benzo[1,2-b:3,4-b′:5,6-b′′] trithiophene 17

According to the procedure given for **9**, 31.6 mg (0.084 mmol, 1.0 eq.) benzo[1,2-b;3,4-b′;5,6-b′′]trithiophene-2,5,8-tricarboxylic and 239.7 mg (0.28 mmol, 3.3 eq.) 5-(3,4,5-tris(hexadecyloxy)phenyl)-2H-tetrazole and 0.2 mL (1.5 mmol, 17.9 eq.) 2,4,6-collidine gave, after stirring for 20 h at 80 °C, and chromatography (SiO_2 (2×18 cm) pure toluene to toluene / ethyl acetate 10:1). In order to separate further by-products, the obtained mixture was adsorbed on aluminum oxide (neutral) and the by-products were eluted with ethyl acetate. Afterwards, the pure product was eluted with chloroform from the stationary phase to yield 85.1 mg (0.03 mmol ≙ 36 %) of a yellowish solid with m. p. = 49 °C (onset, DSC).

^{1}H-NMR (300 MHz, $CDCl_3$): δ [ppm] = 8.12 (s, 1H, H3-BTT), 7.23 (s, 2H, H2-ph, H6-ph), 4.11–4.03 (m, 6H, OCH_2), 1.94–1.75 (m, 6H, CH_2), 1.60–1.51 (m, 6H, CH_2), 1.38–1.26 (m, 72H, CH_2), 0.90–0.85 (m, 9H, CH_3). **^{13}C-NMR (75 MHz, $CDCl_3$):** δ [ppm] = 165.14, 160.00, 153.75, 141.82, 135.10, 131.28, 125.68, 123.60, 117.69, 105.41, 73.74, 69.49, 32.10, 30.62, 29.99, 29.95, 29.92, 29.85, 29.73, 29.61, 29.55, 26.38, 26.32, 22.85, 14.27. **IR (ATR):** $\tilde{\nu}$ [cm^{-1}] = 2952 m, 2916 ss, 2849 ss, 1588 m, 1548 m, 1490 m, 1467 s, 1438 m, 1385 m, 1348 m, 1321 m, 1240 m, 1214 m, 1120 s, 1009 m, 840 m, 757 m, 723 m, 667 m. **MALDI-MS**: 2843.3 calculated for $C_{180}H_{307}N_6O_{12}S_3 + H^+$; found: 2843.1.

Acknowledgements

The authors gratefully acknowledge the Deutsche Forschungsgemeinschaft (DE 515/12-1) for generous funding, Dr. J. Liermann (NMR), U. Kemmer-Jonas (DSC) and Dr. C. Kampf (MS), Dr. D. Schollmeyer (Single Crystal X-Ray Scattering), M. Hehmann for precursor synthesis and the Carl-Zeiss Stiftung for a generous fellowship (N. Tober). Open access funding enabled and organized by Projekt DEAL.

Conflict of Interest

The authors declare no conflict of interest.

Keywords: Discotic liquid crystals · Fluorescence · X-ray diffraction · Heterocycles · Thermotropic mesophase

[1] a) C. Gu, N. Huang, Y. Chen, L. Qin, H. Xu, S. Zhang, F. Li, Y. Ma, D. Jiang, *Angew. Chem. Int. Ed.* **2015**, *54*, 13594–13598; *Angew. Chem.* **2015**, *127*, 13798–13802; b) T. Kashiki, M. Kohara, I. Osaka, E. Miyazaki, K. Takimiya, *J. Org. Chem.* **2011**, *76*, 4061–4070; c) A. Molina-Ontoria, I. Zimmermann, I. Garcia-Benito, P. Gratia, C. Roldán-Carmona, S. Aghazada, M. Graetzel, M. K. Nazeeruddin, N. Martín, *Angew. Chem. Int. Ed.* **2016**, *55*, 6270–6274; *Angew. Chem.* **2016**, *128*, 6378–6382; d) Y. Nicolas, P. Blanchard, E. Levillain, M. Allain, N. Mercier, J. Roncali, *Org. Lett.* **2004**, *6*, 273–276; e) S. Zou, Y. Wang, J. Gao, X. Liu, W. Hao, H. Zhang, H. Zhang, H. Xie, C. Yang, H. Li, W. Hu, *J. Mater. Chem. C* **2014**, *2*, 10011–10016; f) T. Taerum, O. Lukoyanova, R. G. Wylie, D. F. Perepichka, *Org. Lett.* **2009**, *11*, 3230–3233; g) M. Geoghegan, G. Hadziioannou, *Polymer electronics*, Oxford University Press, Oxford **2013, cop. 2013**; h) K. Müllen, G. Wegner, *Electronic materials: The oligomer approach*, Wiley-VCH, Weinheim, New-York **2010**; i) T. A. Skotheim, R. L. Elsenbaumer, J. R. Reynolds, Eds, *Handbook of conducting polymers ; ed. by T. A. Skotheim, R. L. Elsenbaumer, J. R. Reynolds*, M. Dekker, New York, Basel op. **1998**.

[2] a) C. W. Tang, *Appl. Phys. Lett.* **1986**, *48*, 183; b) L. Schmidt-Mende, *Science* **2001**, *293*, 1119–1122; c) I. Seguy, P. Jolinat, P. Destruel, J. Farenc, R. Mamy, H. Bock, J. Ip, T. P. Nguyen, *J. Appl. Phys.* **2001**, *89*, 5442; d) K. Kawata, *The Chemical Record.* **2002**, *2*, 59–80; e) S. Laschat, A. Baro, N. Steinke, F. Giesselmann, C. Hägele, G. Scalia, R. Judele, E. Kapatsina, S. Sauer, A. Schreivogel, M. Tosoni, *Angew. Chem. Int. Ed.* **2007**, *46*, 4832–4887; *Angew. Chem.* **2007**, *119*, 4916–4973; f) B. R. Kaafarani, *Chem. Mater.* **2011**, *23*, 378–396; g) W. Pisula, A. Menon, M. Stepputat, I. Lieberwirth, U. Kolb, A. Tracz, H. Sirringhaus, T. Pakula, K. Müllen, *Adv. Mater.* **2005**, *17*, 684–689; h) D. Adam, P. Schuhmacher, J. Simmerer, L. Häußling, W. Paulus, K. Siemensmeyer, K.-H. Etzbach, H. Ringsdorf, D. Haarer, *Adv. Mater.* **1995**, *7*, 276–280; i) M. Bäker, *Funktionswerkstoffe*, Springer Fachmedien Wiesbaden, Wiesbaden **2014**; j) F. Kaltenbach, Ed, *Transluzente materialien: Glas, kunststoff, metall; Institut für internationale Architektur-Dokumentation*, Munich, Germany **2012**; k) V. P. Shibaev, L. Lam, Eds, *Liquid Crystalline and Mesomorphic Polymers;* Springer, New York, NY, **1994**; l) V. Balzani, G. Bergamini, P. Ceroni, *Angew. Chem. Int. Ed.* **2015**, *54*, 11320–11337; *Angew. Chem.* **2015**, *127*, 11474–11492; m) I. Ata, S. B. Dkhil, M. Pfannmöller, S. Bals, D. Duché, J.-J. Simon, T. Koganezawa, N. Yoshimoto, C. Videlot-Ackermann, O. Margeat, J. Ackermann, P. Bäuerle, *Org. Chem. Front.* **2017**, *4*, 1561–1573; n) N. A. K. Ochs, U. Lewandowska, W. Zajaczkowski, S. Corra, S. Reger, A. Herdlitschka, S. Schmid, W. Pisula, K. Müllen, P. Bäuerle, H. Wennemers, *Chem. Sci.* **2019**, *10*, 5391–5396; o) C. Li, G. Shi, *ACS Appl. Mater. Interfaces* **2013**, *5*, 4503–4510; p) H.-A. Ho, A. Najari, M. Leclerc, *Acc. Chem. Res.* **2008**, *41*, 168–178.

[3] a) A. Demenev, S. H. Eichhorn, T. Taerum, D. F. Perepichka, S. Patwardhan, F. C. Grozema, L. D. A. Siebbeles, R. Klenkler, *Chem. Mater.* **2010**, *22*, 1420–1428; b) G. Kossmehl, G. Schopf, *Polythiophenes – electrically conductive polymers*, Springer, Berlin **1997**.

[4] a) A. Elschner, *PEDOT: Principles and applications of an intrinsically conductive polymer*, CRC Press, Boca Raton, FL **2011**; b) G.-H. Kim, L. Shao, K. Zhang, K. P. Pipe, *Nat. Mater.* **2013**, *12*, 719–723; c) N. Satoh, M. Otsuka, T. Ohki, A. Ohi, Y. Sakurai, Y. Yamashita, T. Mori, *Sci. Technol. Adv. Mater.* **2018**, *19*, 517–525; d) P.-O. Schwartz, M. Pejic, M. Wachtler, P. Bäuerle, *Synth. Met.* **2018**, *243*, 51–57.

[5] a) T. Ikeda, H. Adachi, H. Fueno, K. Tanaka, T. Haino, *J. Org. Chem.* **2017**, *82*, 10062–10069; b) T. Yasuda, T. Shimizu, F. Liu, G. Ungar, T. Kato, *J. Am. Chem. Soc.* **2011**, *133*, 13437–13444; c) A. Pipertzis, G. Zardalidis, K. Wunderlich, M. Klapper, K. Müllen, G. Floudas, *Macromolecules* **2017**, *50*, 1981–1990; d) T. Wohrle, I. Wurzbach, J. Kirres, A. Kostidou, N. Kapernaum, J. Litterscheidt, J. C. Haenle, P. Staffeld, A. Baro, F. Giesselmann, S. Laschat, *Chem. Rev.* **2016**, *116*, 1139–1241; e) D.-G. Kim, Y. H. Kim, T. J. Shin, E. J. Cha, D. S. Kim, B. G. Kim, Y. Yoo, Y. S. Kim, M. H. Yi, J. C. Won, *Chem. Commun.* **2017**, *53*, 8227–8230; f) T. Sakurai, S. Yoneda, S. Sakaguchi, K. Kato, M. Takata, S. Seki, *Macromolecules* **2017**, *50*, 9265–9275; g) L. Cisse, P. Destruel, S. Archambeau, I. Seguy, P. Jolinat, H. Bock, E. Grelet, *Chem. Phys. Lett.* **2009**, *476*, 89–91; h) E. Grelet, H. Bock, *Europhys. Lett.* **2006**, *73*, 712–718.

[6] a) P. Staffeld, M. Kaller, P. Ehni, M. Ebert, S. Laschat, F. Giesselmann, *Crystals* **2019**, *9*, 74; b) I. R. Thompson, M. K. Coe, A. B. Walker, M. Ricci, O. M. Roscioni, C. Zannoni, *Phys. Rev. Materials* **2018**, *2*, 1964; c) A. Gowda, L. Jacob, D. P. Singh, R. Douali, S. Kumar, *ChemistrySelect* **2018**, *3*, 6551–6560; d) S. Kumar, *Liq. Cryst.* **2005**, *32*, 1089–1113.

[7] a) S. Kumar, *Chemistry of discotic liquid crystals: From monomers to polymers*, CRC Press, Boca Raton, FL **2011**; b) H. Detert, *Eur. J. Org. Chem.* **2018**, 4501–4507; c) M. M. Ahmida, S. H. Eichhorn, *ECS Trans.* **2009**, *25*, 1–10; d) X. Feng, W. Pisula, K. Müllen, *Pure Appl. Chem.* **2009**, *81*, 2203–2224; e) R. Cristiano, H. Gallardo, A. J. Bortoluzzi, I. H. Bechtold, C. E. M. Campos, R. L. Longo, *Chem. Commun.* **2008**, 5134–5136.

[8] a) M. Hügel, M. Dechant, N. Scheuring, T. Ghosh, M. Lehmann, *Chem. Eur. J.* **2019**, *25*, 3352–3361; b) M. Lehmann, M. Dechant, M. Lambov, T. Ghosh, *Acc. Chem. Res.* **2019**; c) H. Detert, M. Lehmann, H. Meier, *Materials* **2010**, *3*, 3218–3330.
[9] a) A. Kraft, *Chem. Commun.* **1996**, 77; b) K. Naito, A. Miura, *J. Phys. Chem.* **1993**, *97*, 6240–6248; c) S. K. Pathak, B. Pradhan, R. K. Gupta, M. Gupta, S. K. Pal, A. S. Achalkumar, *J. Mater. Chem. C* **2016**, *4*, 6546–6561; d) N. Röder, T. Marszalek, D. Limbach, W. Pisula, H. Detert, *ChemPhysChem* **2019**, *20*, 463–469; e) B. Roy, N. De, K. C. Majumdar, *Chem. Eur. J.* **2012**, *18*, 14560–14588; f) C.-C. Yang, C.-J. Hsu, P.-T. Chou, H. C. Cheng, Y. O. Su, M.-k. Leung, *J. Phys. Chem. B* **2010**, *114*, 756–768; g) B. Fanady, W. Song, R. Peng, T. Wu, Z. Ge, *Org. Electron.* **2020**, *76*, 105483; h) E. B. Sas, M. Kurban, B. Gündüz, M. Kurt, *Synth. Met.* **2018**, *246*, 39–44; i) H. Detert, E. Sugiono, *Synth. Met.* **2001**, *122*, 19–21.
[10] a) H. Detert, *Synthesis* **1999**, 999–1004; b) D. Limbach, H. Detert, D. Schollmeyer, *IUCrData* **2016**, *1*, 208.
[11] a) S. K. Saha, B. Bhattacharya, U. Sarkar, D. S. Shankar Rao, M. K. Paul, *J. Mol. Liq.* **2017**, *241*, 881–896; b) S. Torgova, S. P. Sreenilayam, Y. P. Panarin, O. Francescangeli, F. Vita, J. K. Vij, E. Pozhidaev, M. Minchenko, C. Ferrero, A. Strigazzi, *Phys. Chem. Chem. Phys.* **2017**, *19*, 22946–22956; c) M. Ferreira, E. Westphal, M. V. Ballottin, I. H. Bechtold, A. J. Bortoluzzi, D. Z. Mezalira, H. Gallardo, *New J. Chem.* **2017**, *41*, 11766–11777; d) S. K. Saha, M. K. Paul, *Liq. Cryst.* **2019**, *46*, 386–396; e) E. Westphal, H. Gallardo, S. Poppe, M. Prehm, C. Tschierske, *J. Mol. Liq.* **2019**, *292*, 111362.
[12] a) H. Tokuhisa, M. Era, T. Tsutsui, *Adv. Mater.* **1998**, *10*, 404–406; b) G. Shanker, M. Prehm, C. Tschierske, *Beilstein J. Org. Chem.* **2012**, *8*, 472–485; c) N. Tober, T. Rieth, M. Lehmann, H. Detert, *Chem. Eur. J.* **2019**, *25*, 15295–15304; d) S. K. Pathak, R. K. Gupta, S. Nath, D. S. S. Rao, S. K. Prasad, A. S. Achalkumar, *J. Mater. Chem. C* **2015**, *3*, 2940–2952; e) B. G. Kim, S. Kim, S. Y. Park, *Tetrahedron Lett.* **2001**, *42*, 2697–2699; f) R. C. Santos, D. M. Pereira de Oliveira, H. Gallardo, *Liq. Cryst.* **2005**, *32*, 7–14; g) J. Han, *J. Mater. Chem. C* **2013**, *1*, 7779; h) J. Han, Z.-Z. Wang, J.-R. Wu, *Liq. Cryst.* **2018**, *45*, 1047–1054; i) N. V. Usol'tseva, O. B. Akopova, A. I. Smirnova, M. I. Kovaleva, N. V. Bumbina, N. V. Zharnikova, *Phase Transitions* **2017**, *90*, 800–807.
[13] a) R.-B. Hou, J.-Y. Su, L.-L. Zhang, D.-F. Li, Y. Xia, *J. Chem. Res.* **2019**, *43*, 3–7; b) K. Asai, T. Ubukata, M. Koshimizu, Y. Fujimoto, T. Yanagida, H. Kawamoto, K. Asai, *J. Mater. Sci. Mater. Electron.* **2019**, *30*, 10211–10216; c) G. Q. Ali, I. H. R. Tomi, *Liq. Cryst.* **2018**, *45*, 421–430; d) M. Homocianu, A. Airinei, C. Hamciuc, A. M. Ipate, *J. Mol. Liq.* **2019**, *281*, 141–149; e) Z. Wei, L. He, Z. Chi, X. Ran, L. Guo, *Spectrochim. Acta Part A* **2019**, *206*, 120–125.
[14] a) T. Rieth, T. Marszalek, W. Pisula, H. Detert, *Chem. Eur. J.* **2014**, *20*, 5000–5006; b) T. Rieth, N. Röder, M. Lehmann, H. Detert, *Chem. Eur. J.* **2018**, *24*, 93–96; c) S. Glang, T. Rieth, D. Borchmann, I. Fortunati, R. Signorini, H. Detert, *Eur. J. Org. Chem.* **2014**, *2014*, 3116–3126.
[15] a) A. Molina-Ontoria, I. Zimmermann, I. Garcia-Benito, P. Gratia, C. Roldán-Carmona, S. Aghazada, M. Graetzel, M. K. Nazeeruddin, N. Martín, *Angew. Chem.* **2016**, *128*, 6378–6382; *Angew. Chem. Int. Ed.* **2016**, *55*, 6270–6274; b) T. Kashiki, S. Shinamura, M. Kohara, E. Miyazaki, K. Takimiya, M. Ikeda, H. Kuwabara, *Org. Lett.* **2009**, *11*, 2473–2475; c) S. Rossi, A. Bisello, R. Cardena, L. Orian, S. Santi, *Eur. J. Org. Chem.* **2017**, *2017*, 5966–5974; d) N. Jayasuriya, J. Kagan, J. E. Owens, E. P. Kornak, D. M. Perrine, *J. Org. Chem.* **1989**, *54*, 4203–4205.
[16] N. Tober, D. Schollmeyer, H. Detert, *IUCrData* **2017**, *2*, 1420.
[17] a) R. Huisgen, J. Sauer, H. J. Sturm, *Angew. Chem.* **1958**, *70*, 272–273; b) R. Huisgen, J. Sauer, H. J. Sturm, J. H. Markgraf, *Chem. Ber.* **1960**, *93*, 2106–2124; c) H. Detert, E. Sugiono, G. Kruse, *J. Phys. Org. Chem.* **2002**, *15*, 638–641.
[18] a) C.-T. Liao, H.-H. Chen, H.-F. Hsu, A. Poloek, H.-H. Yeh, Y. Chi, K.-W. Wang, C.-H. Lai, G.-H. Lee, C.-W. Shih, P.-T. Chou, *Chem. Eur. J.* **2011**, *17*, 546–556; b) A.-A. S. El-Ahl, S. S. Elmorsy, A. H. Elbeheery, F. A. Amer, *Tetrahedron Lett.* **1997**, *38*, 1257–1260; c) G. F. O. Dimroth, *Chem. Chem* **1910**, 2219–2223; d) A. Hetzheim, *Houben Weyl, 4th ed.: VolE8c*, E. Schaumann Ed., Thieme, Stuttgart **1954**.
[19] Deposition Number 2030820 (for **8**) contains the supplementary crystallographic data for this paper. These data are provided free of charge by the joint Cambridge Crystallographic Data Centre and Fachinformationszentrum Karlsruhe Access Structures service www.ccdc.cam.ac.uk/structures.
[20] T. Kashiki, M. Kohara, I. Osaka, E. Miyazaki, K. Takimiya, *J. Org. Chem.* **2011**, *76*, 4061–4070.
[21] B. Wunderlich, *Integration of Fundamental Polymer Science and Technology – 2*, (Eds. P. J. Lemstra, L. A. Kleintjens), Springer Netherlands, Dordrecht **1988**, pp. 329–333.
[22] a) I. Dierking, *Textures of liquid crystals*, Wiley-VCH, Weinheim **2004**; b) S. Kumar, *Liquid crystals: Experimental study of physical properties and phase transitions*, Cambridge University Press, Cambridge **2010**.
[23] P. Scherrer, *Nachr. Ges. Wiss. Goettingen Math.-Phys. Kl.* **1918**, 98–100.
[24] a) M. Lehmann, M. Dechant, M. Holzapfel, A. Schmiedel, C. Lambert, *Angew. Chem. Int. Ed.* **2019**, *58(11)*, 3610–3615; b) O. Kruglova, F. M. Mulder, S. J. Picken, J. Stride, G. J. Kearley, *Physica B* **2004**, *350(1–3, Suppl. 1)*, e1003–e1005.
[25] J. R. Lakowicz, *Principles of fluorescence spectroscopy*, Springer, New York, NY **2010**.

Manuscript received: November 10, 2020
Revised manuscript received: December 23, 2020

FULL PAPERS

C_3-symmetrical stars with a heterocyclic core and a periphery of six to nine alkoxy chains are synthesized via Huisgen reaction. DSC, POM, and TGA give information about the thermal properties of these discotic liquid crystals, XRD enlightens the structures of the very broad mesophases The efficient fluorescence of these discs is positively solvatochromic and strongly influenced by aggregation.

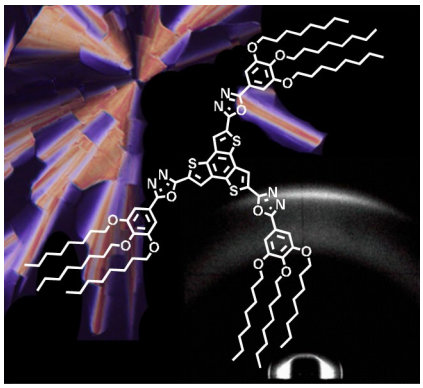

Dr. N. Tober, J. Winter, M. Jochem, Prof. Dr. M. Lehmann, Prof. Dr. H. Detert**